Retired A Stars and Their Companions. IV.
Seven Jovian Exoplanets from Keck Observatory[1]

JOHN ASHER JOHNSON,[2,3] ANDREW W. HOWARD,[4] BRENDAN P. BOWLER,[3] GREGORY W. HENRY,[5] GEOFFREY W. MARCY,[4]
JASON T. WRIGHT,[6] DEBRA A. FISCHER,[7] AND HOWARD ISAACSON[3]

ABSTRACT. We report precise Doppler measurements of seven subgiants from Keck Observatory. All seven stars show variability in their radial velocities consistent with planet-mass companions in Keplerian orbits. The host stars have masses ranging from $1.1 \leq M_\star/M_\odot \leq 1.9$, radii $3.4 \leq R_\star/R_\odot \leq 6.1$, and metallicities $-0.21 \leq [\mathrm{Fe/H}] \leq +0.26$. The planets are all more massive than Jupiter ($M_P \sin i > 1 \; M_{\mathrm{Jup}}$) and have semimajor axes $a > 1$ AU. We present millimagnitude photometry from the T3 0.4 m APT at Fairborn Observatory for five of the targets. Our monitoring shows these stars to be photometrically stable, further strengthening the interpretation of the observed radial velocity variability. The orbital characteristics of the planets thus far discovered around former A-type stars are very different from the properties of planets around dwarf stars of spectral type F, G, and K, and suggests that the formation and migration of planets is a sensitive function of stellar mass. Three of the planetary systems show evidence of long-term, linear trends indicative of additional distant companions. These trends, together with the high planet masses and increased occurrence rate, indicate that A-type stars are very promising targets for direct-imaging surveys.

1. INTRODUCTION

The field of exoplanetary science recently reached a major milestone with the first direct-imaging detections of planetary systems around main-sequence stars.[8] Kalas et al. (2008) detected a single planet-sized object with a semimajor axis $a \approx 120$ AU, orbiting just inside of the dust belt around the nearby, young A4V star Fomalhaut. The young A5V dwarf star HR 8799 is orbited by a system of three substellar objects with semimajor axes $a = \{24, 38, 68\}$ AU (Marois et al. 2008). These remarkable systems share a number of characteristics in common. Both host stars are A-type dwarfs with stellar

masses $>1.5 \; M_\odot$ surrounded by debris disks, the planets are super Jupiters with masses $\lesssim 3 \; M_{\mathrm{Jup}}$, and the companions orbit far from their central stars with unexpectedly large semimajor axes (ranging from 20–120 AU).

That both systems were discovered orbiting A stars might at first seem unlikely, given that A stars make up less than 3% of the stellar population in the Solar neighborhood and because the star-planet contrast ratios are unfavorable compared to systems with fainter, less massive central stars. However, in light of recent discoveries from Doppler-based planet searches of massive stars it is becoming apparent that A dwarfs may in fact be ideal target stars for direct-imaging surveys (Hatzes et al. 2003; Setiawan et al. 2005; Reffert et al. 2006; Sato et al. 2007; Niedzielski et al. 2007; Liu et al. 2008; Döllinger et al. 2009). Measurements of the frequency of giant planets around the "retired" counterparts of A-type dwarfs (subgiants and giants) have found that the occurrence of Jovian planets scales with stellar mass: A-type stars ($M_\star \gtrsim 1.5 \; M_\odot$) are at least 5 times more likely than M dwarfs to harbor a giant planet (Johnson et al. 2007a; Bowler et al. 2010; Johnson et al. 2010). And just like the current sample of imaged planets, Doppler-detected planets around retired A stars are more massive (Lovis & Mayor 2007) and orbit farther from their stars than do planets found around Sun-like, F, G, and K (FGK) dwarfs (Johnson et al. 2007b; Sato et al. 2008).

Indeed, there is strong evidence that the orbital characteristics of planets around A stars are drawn from a statistical parent population that is distinct from those of planets around FGK dwarfs. Bowler et al. (2010) performed a statistical analysis

---

[2] Department of Astrophysics, California Institute of Technology, Pasadena, CA 91125; NASA Exoplanet Science Institute (NExScI); johnjohn@astro.berkeley.edu.

[3] Institute for Astronomy, University of Hawai'i, Honolulu, HI 96822.

[4] Department of Astronomy, University of California, Berkeley, CA 94720.

[5] Center of Excellence in Information Systems, Tennessee State University, Nashville, TN 37209.

[6] Department of Astronomy & Astrophysics, Pennsylvania State University, University Park, PA 16802.

[7] Department of Astronomy, Yale University, New Haven, CT 06511.

[8] The planet candidate around the A-type star β Pic announced by Lagrange et al. (2009b) has not yet been confirmed by proper motion (Fitzgerald et al. 2009; Lagrange et al. 2009a). Similarly, there exists no proper motion follow-up of the faint object imaged around 1RXS J160929.1-210524 (Lafrenière et al. 2008).

of planets detected in the Lick Subgiants Survey, which comprises 31 massive stars ($M_\star \gtrsim 1.5\ M_\odot$) monitored for the past 5 yr. The mass-period distribution of exoplanets around FGK dwarfs is typically described by a double–power-law relationship, with the frequency of planets rising toward lower masses and remaining flat in logarithmic semimajor-axis bins from ∼0.05 AU to ∼5 AU (Tabachnik & Tremaine 2002; Lineweaver & Grether 2003; Cumming et al. 2008; Johnson 2009). Based on the 7 planet detections from the Lick survey, Bowler et al. concluded that the power-law indices of the distribution of planets around A stars and Sun-like stars differ at the 4σ level; the planets in their sample all have $M_P \sin i >$1.5 $M_{\rm Jup}$ and none orbit within 1 AU. However, their small sample size precluded a determination of the exact shape of the mass-period distribution. Fortunately, given the $26^{+9}_{-8}\%$ occurrence rate measured from the Lick survey, it will not take long to build a statistical ensemble comparable to the collection of planets around less massive stars.

To increase the collection of planets detected around massive stars, and to study the relationships among the characteristics of stars and the properties of their planets, we are conducting a survey of massive subgiants at Keck and Lick Observatories. The decreased rotation rates and cooler surface temperatures of these evolved stars make them much more ideal Doppler-survey targets compared to their massive main-sequence progenitors (Galland et al. 2005). The observed effects of stellar mass on the properties of planets have important implications for planet formation modeling (Ida & Lin 2005; Kennedy & Kenyon 2008; Kretke et al. 2009; Currie 2009; Dodson-Robinson et al. 2009); the interpretation of observed structural features in the disks around massive stars (Wyatt et al. 1999; Quillen 2006; Brittain et al. 2009); and the planning of current and future planet search efforts, such as the Gemini Planet Imager (GPI; Macintosh et al. 2008), Spectro-Polarimetric High-contrast Exoplanets REsearch (SPHERE; Claudi et al. 2006), the Near-Infrared Coronographic Imager (NICI; Artigau et al. 2008), and *Project 1640* (Hinkley et al. 2008). Our Lick survey has resulted in the discovery of seven new Jovian planets orbiting evolved stars more massive than the Sun (Johnson et al. 2006, 2007b, 2008; Peek et al. 2009; Bowler et al. 2010). In this contribution, we present the first seven planets discovered in the expanded Keck survey.

2. A DOPPLER SURVEY OF SUBGIANTS AT KECK OBSERVATORY

2.1. Target Selection

We are monitoring the radial velocities (RV) of a sample of 500 evolved stars at Keck Observatory. The Keck program expands upon our Doppler survey of 120 subgiants at Lick Observatory, which has been ongoing since 2004 (Johnson et al. 2006; Peek et al. 2009). The stars in the Lick program have now been folded into the Keck target list and that subset of brighter subgiants ($V < 7.25$) is currently monitored at both observatories. We began the Keck survey in 2007 April for the majority of our target stars, and a handful of stars were part of the original Keck planet search sample dating as far back as 1997 (Marcy et al. 2008).

We selected the targets for the expanded Keck survey from the *Hipparcos* catalog based on the criteria $1.8 < M_V < 3.0$, $0.8 < B - V < 1.1$, and $V \lesssim 8.5$ (ESA 1997; van Leeuwen 2007). We chose the red cutoff to avoid red giants, the majority of which are already monitored by other planet search programs and are known to exhibit velocity jitter >10 m s^{-1} (Sato et al. 2005; Hekker et al. 2006; Niedzielski et al. 2009). The lower M_V restriction avoids Cepheid variables, and the upper limit excludes stars with masses less than 1.3 $M_\odot$ when compared to the Solar-metallicity ([Fe/H = 0]) stellar model tracks of Girardi et al. (2002). We also excluded stars in the clump region ($B - V > 0.8$, $M_V < 2.0$) to avoid the closely-spaced and often overlapping mass tracks in that region of the theoretical H-R diagram.

2.2. Stellar Properties

Atmospheric parameters of the target stars are estimated from iodine-free, "template" spectra using the LTE spectroscopic analysis package *Spectroscopy Made Easy* (SME; Valenti & Piskunov 1996), as described by Valenti & Fischer (2005) and Fischer & Valenti (2005). To constrain the low surface gravities of the evolved stars, we used the iterative scheme of Valenti et al. (2009), which ties the SME-derived value of log g to the gravity inferred from the Yonsei-Yale (Y^2; Yi et al. 2004) stellar model grids. The analysis yields a best-fit estimate of $T_{\rm eff}$, log g, [Fe/H], and $V_{\rm rot} \sin i$. The properties of the majority of our targets from Lick and Keck are listed in the fourth edition of the Spectroscopic Properties of Cool Stars Catalog (SPOCS IV; Johnson et al. 2010, in prep). We adopt the SME parameter uncertainties described in the error analysis of Valenti & Fischer (2005).

The luminosity of each star is estimated from the apparent V-band magnitude, the bolometric correction (Flower 1996), and the parallax from *Hipparcos* (van Leeuwen 2007). From $T_{\rm eff}$ and luminosity, we determine the stellar mass, radius, and an age estimate by associating those observed properties with a model from the Y^2 stellar interior calculations (Yi et al. 2004). We also measure the chromospheric emission in the Ca II line cores (Wright et al. 2004; Isaacson 2009), providing an $S_{\rm HK}$ value on the Mt. Wilson system, which we convert to log $R'_{\rm HK}$ as per Noyes et al. (1984).

The stellar properties of the seven stars presented herein are summarized in Table 1.

TABLE 1
STELLAR PARAMETERS

Parameter	HD 4313	HD 95089	HD 181342	HD 206610	HD 180902	HD 136418	HD 212771
V	7.83	7.92	7.55	8.34	7.78	7.88	7.60
$B - V$	0.96	0.94	1.02	1.01	0.94	0.93	0.88
Distance (pc)	137 (14)	139 (16)	110.6 (7.5)	194 (36)	110 (10)	98.2 (5.6)	131 (14)
M_V	2.2 (0.3)	2.1 (0.3)	2.2 (0.2)	2.2 (0.4)	2.5 (0.3)	2.7 (0.2)	2.2 (0.3)
[Fe/H]	+0.14 (0.03)	+0.05 (0.03)	+0.26 (0.03)	+0.14 (0.03)	0.04 (0.03)	−0.07 (0.03)	−0.21 (0.03)
$T_{\rm eff}$ (K)	5035 (44)	5002 (44)	5014 (44)	4874 (44)	5030 (44)	5071 (44)	5121 (44)
$V_{\rm rot} \sin i$ (km s^{-1})	2.76 (0.5)	2.74 (0.5)	3.04 (0.5)	2.57 (0.5)	2.88 (0.5)	0.17 (0.5)	2.63 (0.5)
$\log g$	3.4 (0.06)	3.4 (0.06)	3.4 (0.06)	3.3 (0.06)	3.5 (0.06)	3.6 (0.06)	3.5 (0.06)
M_* $(M_\odot)$	1.72 (0.12)	1.58 (0.11)	1.84 (0.13)	1.56 (0.11)	1.52 (0.11)	1.33 (0.09)	1.15 (0.08)
R_* $(R_\odot)$	4.9 (0.1)	4.9 (0.1)	4.6 (0.1)	6.1 (0.1)	4.1 (0.1)	3.4 (0.1)	5.0 (0.1)
L_* $(R_\odot)$	14.1 (0.5)	13.5 (0.5)	12.0 (0.5)	18.9 (0.6)	9.4 (0.5)	6.8 (0.5)	15.4 (0.5)
Age (Gyr)	2.0 (0.5)	2.5 (0.9)	1.8 (0.4)	3 (1)	2.8 (0.7)	4 (1)	6 (2)
$S_{\rm HK}$	0.12	0.13	0.12	0.14	0.15	0.14	0.16
$\log R'_{\rm HK}$	−5.27	−5.22	−5.31	−5.23	−5.14	−5.19	−5.09

3. OBSERVATIONS AND ANALYSIS

3.1. Keck Spectra and Doppler Analysis

We obtained spectroscopic observations at Keck Observatory using the HIRES spectrometer with a resolution of $R \approx 55,000$ with the B5 decker (0.86″ width) and red cross-disperser (Vogt et al. 1994). We use the HIRES exposure meter to ensure that all observations receive uniform flux levels independent of atmospheric transparency variations, and to provide the photon-weighted exposure midpoint which is used for the barycentric correction. Under nominal atmospheric conditions, a $V = 8$ target requires an exposure time of 90 s and results in a signal-to-noise ratio of 190 at 5500 Å.

The spectroscopic observations are made through a temperature-controlled Pyrex cell containing gaseous iodine, which is placed at the entrance slit of the spectrometer. The dense set of narrow molecular lines imprinted on each stellar spectrum from 5000 Å to 6000 Å provides a robust, simultaneous wavelength calibration for each observation, as well as information about the shape of the spectrometer's instrumental response (Marcy & Butler 1992). Doppler shifts are measured from each spectrum using the modeling procedure described by Butler et al. (1996). The instrumental uncertainty of each measurement is estimated based on the weighted standard deviation of the mean Doppler shift measured from each of ≈ 700 2 Å spectral chunks. In a few instances, we made two or more successive observations of the same star and binned the velocities (in 2 hr time intervals), thereby reducing the associated measurement uncertainty.

3.2. Photometric Measurements

We also acquired brightness measurements of five of the seven planetary candidate host stars with the T3 0.4 m automatic photometric telescope (APT) at Fairborn Observatory. T3 observed each program star differentially with respect to two comparisons stars in the following sequence, termed a group observation: K,S,C,V,C,V,C,V,C,S,K, where K is a check (or secondary comparison) star, C is the primary comparison star, V is the program (normally a variable) star, and S is a sky reading. Three $V - C$ and two $K - C$ differential magnitudes are computed from each sequence and averaged to create group means. Group-mean differential magnitudes with internal standard deviations greater than 0.01 mag were rejected to eliminate the observations taken under nonphotometric conditions. The surviving group means were corrected for differential extinction with nightly extinction coefficients, transformed to the Johnson system with yearly-mean transformation coefficients, and treated as single observations thereafter. The typical precision of a single group-mean observation from T3, as measured for pairs of constant stars, is ∼0.004–0.005 mag (e.g., Henry et al. 2000 Tables 2–3). Further information on the operation of the T3 APT can be found in Henry et al. (1995b, 1995a) and Eaton et al. (2003).

Our photometric observations are useful for eliminating potential false positives from the sample of new planets. Queloz et al. (2001) and Paulson et al. (2004) have demonstrated how rotational modulation in the visibility of starspots on active stars can result in periodic radial velocity variations and potentially lead to erroneous planetary detections. Photometric results for the stars in the present sample are given in Table 2. Columns (7)–(10) give the standard deviations of the $V - C$ and $K - C$ differential magnitudes in the B and V passbands with the 3σ outliers removed. With the exception of HD 206610, all of the standard deviations are small and approximately equal to the measurement precision of the telescope.

For HD 206610, the standard deviations of the four data sets $(V - C)_B$, $(V - C)_V$, $(K - C)_B$, and $(K - C)_V$ are all larger than 0.01 mag and indicate photometric variability. Periodogram analyses revealed that all four data sets have a photometric period of 0.09 day and an amplitude of ∼0.03 mag. Thus, the variability must arise from HD 206610's primary comparison

TABLE 2
SUMMARY OF PHOTOMETRIC OBSERVATIONS FROM FAIRBORN OBSERVATORY

Program Star (1)	Comparison Star (2)	Check Star (3)	Date Range (HJD−2,440,000) (4)	Duration (days) (5)	N_{obs} (6)	$\sigma(V-C)_B$ (mag) (7)	$\sigma(V-C)_V$ (mag) (8)	$\sigma(K-C)_B$ (mag) (9)	$\sigma(K-C)_V$ (mag) (10)	Variability (11)
HD 4313 ……	HD 4627	HD 4526	54756–55222	466	188	0.0039	0.0046	0.0038	0.0056	Constant
HD 95089 ……	HD 94401	HD 93102	55139–55237	98	58	0.0056	0.0059	0.0045	0.0064	Constant
HD 180902 ……	HD 179949	HD 181240	55122–55126	4	3	0.0032	0.0031	0.0010	0.0056	Constant?
HD 206610 ……	HD 205318	HD 208703	54756–55170	414	88	0.0183[a]	0.0140[a]	0.0172	0.0124	Constant
HD 212771 ……	HD 212270	HD 213198	55119–55170	51	60	0.0043	0.0048	0.0051	0.0065	Constant

[a] Comparison star HD 205318 is variable in brightness, so we recomputed the standard deviations of the program star from the $(V-K)_B$ and $(V-K)_V$ differential magnitudes, and find them to be 0.0066 mag and 0.0067 mag in B and V, respectively.

star $(C = \mathrm{HD}\,205318)$, which is included in all four data sets. Given its period, amplitude, and early-F spectral class, it is probably a new δ Scuti star. We computed new differential magnitudes for HD 206610 using the check star (K) to form the variable minus check data sets $(V - K)_B$ and $(V - K)_V$. The standard deviations of these two data sets are 0.0066 mag and 0.0067 mag, respectively.

Therefore, all five of the planetary candidate stars in Table 2 are photometrically constant to the approximate limit of the APT observations. The measured photometric stability supports the planetary interpretation of the radial velocity variations. The two stars that we did not observe photometrically, HD 136418 and and HD 181342, have similar masses, colors, and activity levels (Table 2) as the five stars we did observe and so are likely to be photometrically constant as well.

3.3. Orbit Analysis

For each star we performed a thorough search of the measured velocities for the best-fitting, single-planet Keplerian orbital model using the partially-linearized, least-squares fitting procedure described in Wright & Howard (2009) and implemented in the IDL package RVLIN.[9] Before searching for a best-fitting solution, we increased the measurement uncertainties by including an error contribution due to stellar "jitter." The jitter accounts for any unmodeled noise sources intrinsic to the star such as rotational modulation of surface inhomogeneities and pulsation (Saar et al. 1998; Wright 2005; Makarov et al. 2009; Lagrange et al. 2010).

We estimate the jitter for our subgiants based on the velocity variability of a sample of "stable" stars, for which we have obtained >4 observations over a time span greater than 2 yr. These stars do not show evidence of an orbital companion, except in a few cases where the stars exhibit a linear trend. In those cases we remove the trend using a linear fit and consider the scatter in the residuals. Figure 1 shows the distribution of RVs for all 72 stable stars, comprising 382 measurements. We fit a Gaussian function to the distribution with a width $\sigma = 5.1$ m s^{-1}. The measurement uncertainties, shown in the lower panel, span 0.6–2.5 m s^{-1}, with a median value of 1.2 m s^{-1}. We subtracted this median internal error in quadrature from the measured width of the distribution of RVs to produce a jitter estimate of 4.95 m s^{-1}. In the analysis of each star's RV time series we round this value up and adopt a uniform jitter estimate of 5 m s^{-1}, which we add in quadrature to the measurement uncertainties before searching for the best-fitting orbit.

After identifying the best-fitting model, we use a Markov-Chain Monte Carlo (MCMC) algorithm to estimate the parameter uncertainties (see, e.g., Ford 2005; Winn et al. 2007). MCMC is a Bayesian inference technique that uses the data to explore the shape of the likelihood function for each para-
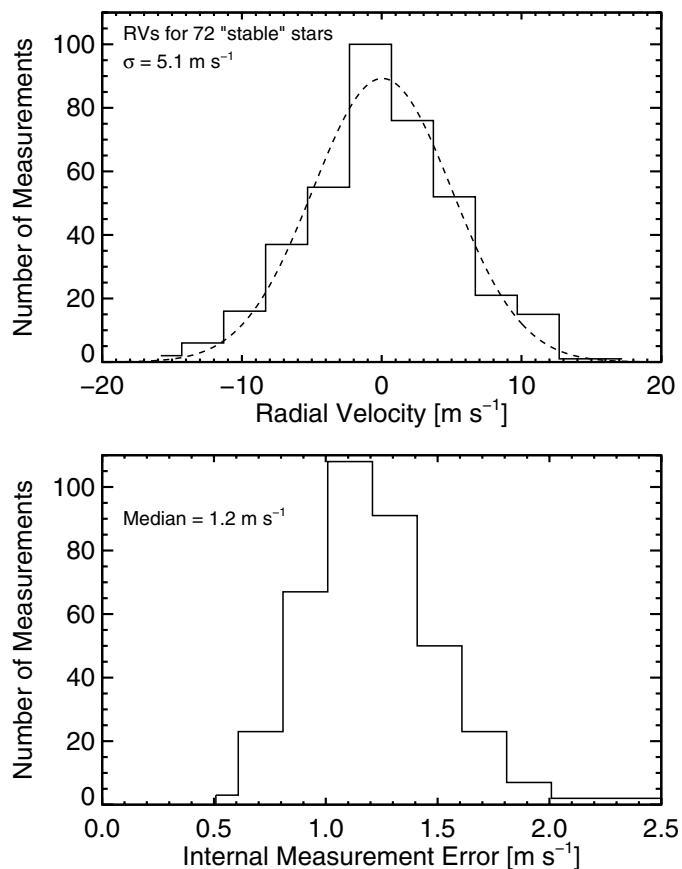
[9] At http://exoplanets.org/code/.

FIG. 1.—*Top.* Distribution of RVs for 72 standard stars, comprising a total of 382 measurements. The *dashed line* shows the best-fitting Gaussian with a width $\sigma = 5.1$ m s^{-1}. *Bottom.* Distribution of internal measurement uncertainties for 382 RV measurements. The median is 1.2 m s^{-1}. Together with the distribution of RVs in the top panel, this provides us with a jitter estimate of 5 m s^{-1}, which we apply to all of the stars presented herein.

meter of an input model. At each step, one parameter is selected at random and altered by drawing a random variate from a normal distribution. If the resulting χ^2 value for the new trial orbit is smaller than the previous χ^2 value, then the trial orbital parameters are added to the chain. If not, then the probability of adopting the new value is set by the ratio of the probabilities from the previous and current trial steps. If the current trial is rejected then the parameters from the previous step are adopted.

We alter the standard deviations of the random parameter variates so that the acceptance rates are between 20% and 40%. The initial parameters are chosen from the best-fitting orbital solutions derived using the least-squares method described here, and each chain is run for 10^7 steps. The initial 10% of the chains are excluded from the final estimation of parameter uncertainties to ensure uniform convergence. We verify that convergence is reached by running five shorter chains with 10^6 steps and checking that the Gelman-Rubin statistic (Gelman

& Rubin 1992) for each parameter is near unity ($\lesssim 1.02$) and that a visual inspection of the history plots suggests stability.

The resulting "chains" of parameters form the posterior probability distribution, from which we select the 15.9 and 84.1 percentile levels in the cumulative distributions as the "1σ" confidence limits. In most cases, the posterior probability distributions were approximately Gaussian.

3.4. Testing RV Trends

We use the Bayesian Information Criterion (BIC; Schwarz 1978; Liddle 2004) and the MCMC posterior probability density functions (pdf) to determine whether there is evidence for a linear velocity trend (Bowler et al. 2010). The BIC rewards better-fitting models but penalizes overly complex models, and is given by

$$\mathrm{BIC} \equiv -2 \ln \mathcal{L}_{\max} + k \ln N, \qquad (1)$$

where $\mathcal{L}_{\max} \propto \exp(-\chi^2_{\min}/2)$ is the maximum likelihood for a particular model with k free parameters and N data points.[10] A difference of $\gtrsim 2$ between BIC values with and without a trend indicates that there is sufficient evidence for a more complex model (Kuha 2004).

We also use the MCMC-derived pdf for the velocity trend parameter to estimate the probability that a trend is actually present in the data. If the 99.7 percentile of the pdf lies above or below $0 \mathrm{~m~s}^{-1} \mathrm{~yr}^{-1}$ then we adopt the model with the trend. The BIC and MCMC methods yield consistent results for the planet candidates described in § 4.

3.5. False-Alarm Evaluation

For each planet candidate we consider the null–hypothesis that the apparent periodicity arose by chance from larger-than-expected radial velocity fluctuations and sparse sampling. We test this possibility by calculating the false-alarm probability (FAP) based on the goodness-of-fit statistic $\Delta\chi^2_\nu$ (Howard et al. 2009; Marcy et al. 2005; Cumming 2004), which is the difference between two values of χ^2_ν: one from the single-planet Keplerian fit and one from the fit of a linear trend to the data. Each trial is constructed by keeping the times of observation fixed and scrambling the measurements, with replacement. We record the $\Delta\chi^2_\nu$ value after each trial and repeat this process for 10,000 trial data sets. For the ensemble set we compare the resulting distribution of $\Delta\chi^2_\nu$ to the value from the fit to the original data. The planets presented in § 4 all have FAP <0.001, corresponding to <0.5 false alarms for our sample of 500 stars.

---

[10] The relationship between $\mathcal{L}_{\max}$ and $\chi^2_{\min}$ is only valid under the assumption that the errors are described by a Gaussian, which is approximately valid for our analyses.
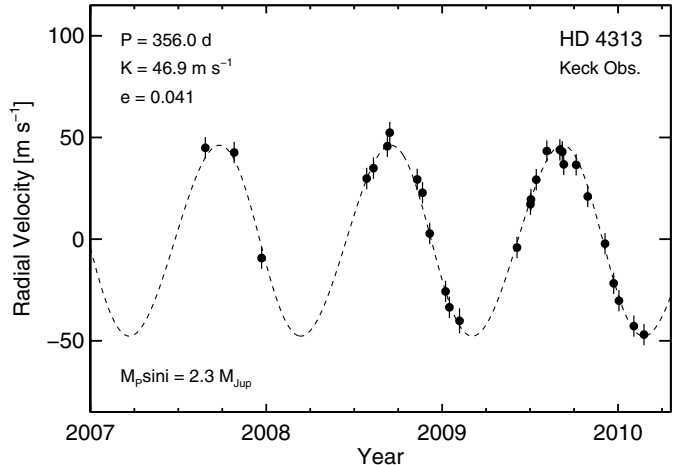

FIG. 2.—Relative RVs of HD 4313 measured at Keck Observatory. The error bars are the quadrature sum of the internal measurement uncertainties and 5 m s^{-1} of jitter. The *dashed line* shows the best-fitting orbit solution of a single Keplerian orbit. The solution results in residuals with an rms scatter of 3.7 m s^{-1} and $\sqrt{\chi^2_\nu} = 0.79$.

4. RESULTS

We have detected seven new Jovian planets orbiting evolved, subgiant stars. The RV time series of each host star is plotted in Figures 2–8, where the error bars show the quadrature sum of the internal errors and the jitter estimate of 5 m s^{-1}, as described in § 3.3. The RV measurements for each star are listed in Tables 3–9, together with the Julian date of observation and the internal measurement uncertainties (without jitter). The best-fitting orbital parameters and physical characteristics of the
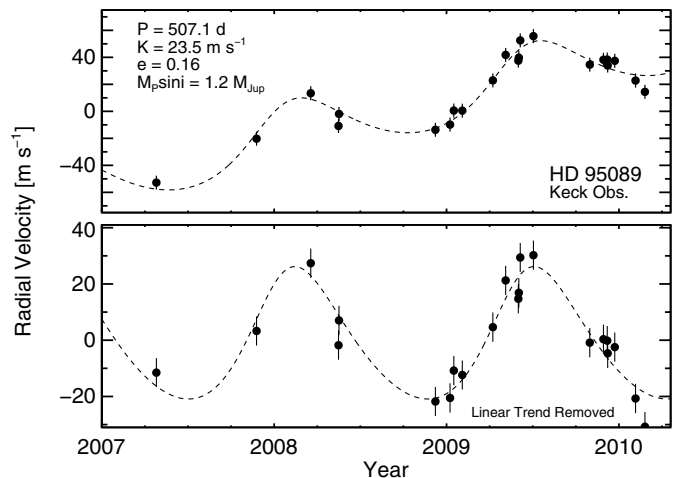

FIG. 3.—Relative RVs of HD 95089 measured at Keck Observatory. The error bars are the quadrature sum of the internal measurement uncertainties and 5 m s^{-1} of jitter. The *dashed line* shows the best-fitting orbit solution of a single Keplerian orbit plus a linear trend ($dv/dt = 30.9 \pm 1.9 \mathrm{~m~s}^{-1} \mathrm{~yr}^{-1}$). The solution results in residuals with an rms scatter of 5.7 m s^{-1} and $\sqrt{\chi^2_\nu} = 1.32$. The *lower panel* shows the RVs with the linear trend removed.

FIG. 4.—Relative RVs of HD 181342 measured at Keck Observatory. The error bars are the quadrature sum of the internal measurement uncertainties and 5 m s^{-1} of jitter. The *dashed line* shows the best-fitting orbit solution of a single Keplerian orbit. The solution results in residuals with an rms scatter of 4.7 m s^{-1} and $\sqrt{\chi_\nu^2} = 1.14$.
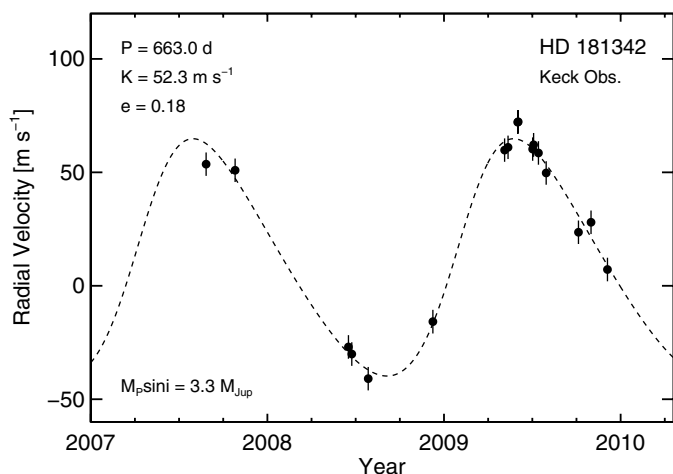

FIG. 6.—Relative RVs of HD 180902 measured at Keck Observatory. The error bars are the quadrature sum of the internal measurement uncertainties and 5 m s^{-1} of jitter. The *dashed line* shows the best-fitting orbit solution of a single Keplerian orbit plus a linear trend ($dv/dt = 135.4 \pm 3.5$ m s^{-1} yr^{-1}). The solution results in residuals with an rms scatter of 3.3 m s^{-1} and $\sqrt{\chi_\nu^2} = 0.98$. The *lower panel* shows the RVs with the linear trend removed.

planets are summarized in Table 10, along with their uncertainties. When appropriate we list notes for some of the individual planetary systems.

HD 95089, HD 136418, HD 180902.—The orbit models for these three stars include linear trends. We interpret the linear trend as a second orbital companion with a period longer than the time baseline of the observations.

HD 181342.—The time sampling of HD 181342 is sparser than most of the the other stars presented in this work. However,

the large amplitude of the variations and observations clustered near the quadrature points result in a well-defined χ_ν^2 minimum in the orbital parameter space. The FAP for the orbit solution is 0.0064%.

HD 212771.—This low-mass subgiant has a mass $M_\star = 1.15\ M_\odot$, indicating that it had a spectral type of early G to late F while on the main sequence. In addition to being one
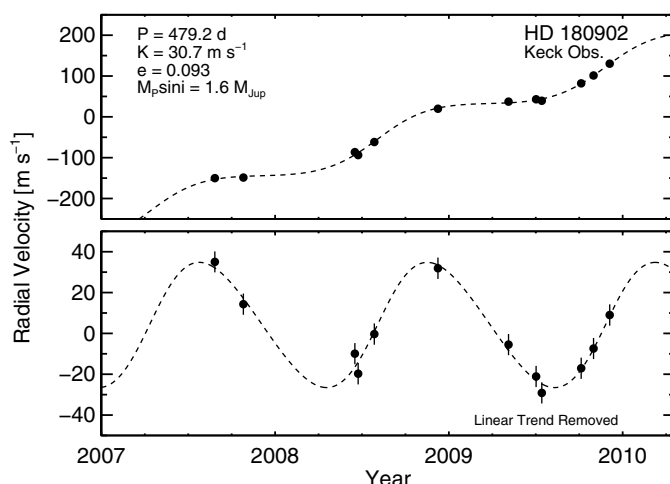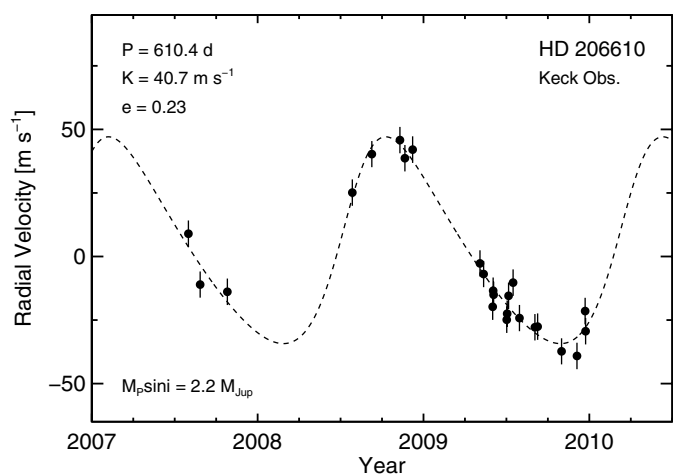

FIG. 5.—Relative RVs of HD 206610 measured at Keck Observatory. The error bars are the quadrature sum of the internal measurement uncertainties and 5 m s^{-1} of jitter. The *dashed line* shows the best-fitting orbit solution of a single Keplerian orbit. The solution results in residuals with an rms scatter of 4.8 m s^{-1} and $\sqrt{\chi_\nu^2} = 1.06$.
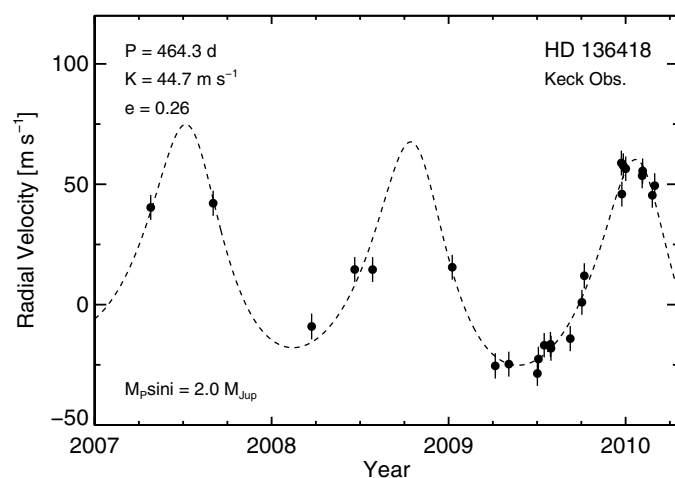
FIG. 7.—Relative RVs of HD 136418 measured at Keck Observatory. The error bars are the quadrature sum of the internal measurement uncertainties and 5 m s^{-1} of jitter. The *dashed line* shows the best-fitting orbit solution of a single Keplerian orbit plus a linear trend ($dv/dt = -5.3 \pm 1.7$ m s^{-1} yr^{-1}). The solution results in residuals with an rms scatter of 5.0 m s^{-1} and $\sqrt{\chi_\nu^2} = 1.15$. HD 136418 has a mass $M_\star = 1.33\ M_\odot$, making it a former F-type star.

FIG. 8.—Relative radial velocity measurements of HD 212771. The error bars are the quadrature sum of the internal measurement uncertainties and 5 m s^{-1} of jitter. The dashed line shows the best-fitting orbit solution of a single Keplerian orbit. The solution results in residuals with 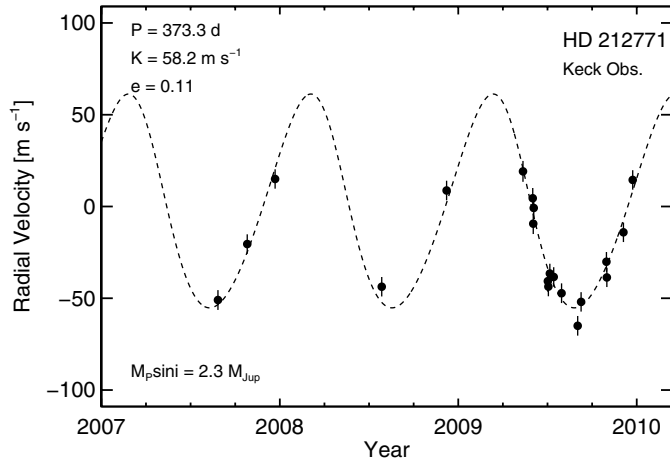an rms scatter of 5.8 m s^{-1} and $\sqrt{\chi_\nu^2} = 1.29$. HD 212771 has a mass $M_\star = 1.15 \ M_\odot$, indicating that it was either an early G or late F star when it was on the main sequence.

of our least massive targets, HD 212771 is also one of the most metal-poor stars in the Keck sample $[\text{Fe/H}] = -0.21$. Poor RV coverage near velocity maximum due to the nearly annual signal may result in a relatively weak constraint on its eccentricity. We quote the upper limit (95% confidence) in Table 10.

TABLE 3
RADIAL VELOCITIES FOR HD 4313

JD−2,440,000	RV (m s^{-1})	Uncertainty (m s^{-1})
14339.932	23.92	1.57
14399.842	21.61	1.59
14456.806	−30.29	1.61
14675.006	8.82	1.71
14689.004	13.91	1.60
14717.945	24.71	1.53
14722.895	31.39	1.60
14779.854	8.37	1.70
14790.889	1.82	1.64
14805.807	−18.24	1.54
14838.768	−46.70	1.61
14846.745	−54.50	1.69
14867.754	−61.16	3.56
14987.118	−25.11	1.69
15015.049	−3.83	1.54
15016.081	−1.47	1.41
15027.089	8.26	1.61
15049.038	22.34	1.56
15076.091	22.90	1.60
15081.091	21.97	1.55
15084.143	15.79	1.60
15109.955	15.55	1.63
15133.975	0.00	1.60
15169.860	−23.21	1.57
15187.855	−42.72	1.55
15198.771	−51.25	1.55
15229.722	−63.75	1.43
15250.713	−67.93	1.50

TABLE 4
RADIAL VELOCITIES FOR HD 95089

JD−2,440,000	RV (m s^{-1})	Uncertainty (m s^{-1})
14216.851	−11.35	1.26
14429.126	3.46	1.35
14543.962	27.54	1.44
14602.807	−1.61	1.19
14603.793	7.19	1.39
14808.056	−21.62	1.25
14839.102	−20.36	1.49
14847.054	−10.63	1.52
14865.063	−12.19	1.27
14929.816	4.82	1.47
14956.912	21.43	1.36
14983.770	14.90	1.40
14984.829	17.03	1.50
14987.835	29.57	1.28
15015.761	30.40	1.33
15135.149	−0.70	1.42
15164.109	0.53	1.34
15172.146	0.00	1.45
15173.095	−4.48	1.47
15188.103	−2.29	1.42
15232.135	−20.55	1.49
15252.034	−30.59	1.53

TABLE 5
RADIAL VELOCITIES FOR HD 181342

JD−2,440,000	RV (m s^{-1})	Uncertainty (m s^{-1})
14339.768	2.69	1.28
14399.741	0.00	1.33
14634.063	−77.87	1.43
14641.000	−81.00	1.44
14674.973	−91.85	1.32
14808.687	−66.72	1.50
14957.027	8.89	1.28
14964.119	10.11	1.29
14984.083	21.20	1.31
14985.112	21.37	1.35
15015.014	9.33	1.22
15016.963	11.24	1.41
15026.967	7.63	1.38
15042.963	−1.18	1.38
15109.749	−27.32	1.34
15135.743	−22.92	1.38
15169.686	−43.74	1.42

TABLE 6
RADIAL VELOCITIES FOR HD 206610

JD−2,440,000	RV (m s^{-1})	Uncertainty (m s^{-1})
14313.980	22.85	1.48
14339.843	2.84	1.25
14399.759	0.00	1.48
14674.964	39.03	1.42
14717.919	54.16	1.20
14779.822	59.68	1.36
14790.746	52.55	1.42
14807.783	55.93	1.57
14956.102	11.16	1.28
14964.118	6.98	1.26
14984.082	−5.90	1.27
14985.111	0.42	1.43
14986.113	−1.17	1.27
15015.022	−11.00	1.36
15015.956	−8.62	1.37
15019.066	−1.59	1.47
15029.011	3.61	1.46
15043.058	−10.34	1.31
15077.058	−13.95	1.40
15083.055	−13.70	1.41
15135.761	−23.43	1.13
15169.700	−25.24	1.46
15187.696	−7.58	1.50
15188.691	−15.51	1.40

TABLE 8
RADIAL VELOCITIES FOR HD 136418

JD−2,440,000	RV (m s^{-1})	Uncertainty (m s^{-1})
14216.954	25.79	1.27
14345.803	27.56	1.50
14549.041	−23.63	1.97
14637.956	0.03	1.26
14674.797	0.00	1.32
14839.165	0.97	1.21
14927.948	−40.01	1.66
14955.930	−39.28	1.38
15014.866	−43.17	1.21
15016.982	−37.15	1.13
15028.959	−31.44	0.96
15041.838	−31.07	1.26
15042.875	−32.70	1.33
15082.729	−28.68	1.46
15106.719	−13.60	1.43
15111.702	−2.58	1.49
15188.168	44.27	1.27
15189.147	31.37	1.37
15192.148	43.12	1.31
15197.173	41.88	0.99
15231.100	38.97	1.41
15232.083	40.97	1.32
15252.046	30.85	1.26
15256.997	34.86	1.34

5. SUMMARY AND DISCUSSION

We report the detection of seven new Jovian planets orbiting evolved stars. These detections come from the sample of subgiants that we are monitoring at Lick and Keck Observatories. The host stars have masses in the range 1.15 $M_\odot$ to 1.9 $M_\odot$, radii $3.4 \leq R_\star/R_\odot \leq 6.1$, and metallicities $-0.21 \leq [\text{Fe/H}] \leq +0.26$. Five of the host stars have masses $M_\star > 1.5 \ M_\odot$, and are therefore the evolved counterparts of the A-type stars. We also derived a jitter estimate for our sample

of evolved stars and find that subgiants are typically stable to within 5 m s^{-1}. The observed jitter of subgiants makes them uniquely stable Doppler targets among massive, evolved stars (Fischer et al. 2003; Hekker et al. 2006).

TABLE 7
RADIAL VELOCITIES FOR HD 180902

JD−2,440,000	RV (m s^{-1})	Uncertainty (m s^{-1})
14339.767	40.51	1.17
14399.740	19.80	1.37
14634.062	−4.44	1.37
14640.998	−14.25	1.59
14674.972	5.16	1.51
14808.686	37.39	1.56
14957.026	0.00	1.44
15015.013	−15.62	1.39
15026.965	−23.67	1.33
15109.748	−11.60	1.45
15135.741	−1.92	1.33
15169.685	14.50	1.51

TABLE 9
RADIAL VELOCITIES FOR HD 212771

JD−2,440,000	RV (m s^{-1})	Uncertainty (m s^{-1})
14339.830	−20.86	2.03
14399.773	9.64	1.79
14456.785	45.09	1.68
14675.025	−13.62	1.77
14807.780	38.82	1.84
14964.124	49.23	2.70
14984.088	34.58	2.51
14985.116	20.73	2.62
14986.117	29.29	2.77
15015.023	−10.59	2.63
15016.078	−13.55	1.63
15019.080	−6.43	1.88
15027.008	−8.30	1.80
15043.060	−17.15	1.96
15076.073	−34.91	1.91
15083.064	−21.87	1.74
15134.930	0.00	1.74
15135.765	−8.56	1.52
15169.702	16.03	1.77
15188.695	44.57	1.77

TABLE 10

ORBITAL PARAMETERS

Parameter	HD 4313[b]	HD 95089[b]	HD 181342[b]	HD 206610[b]	HD 180902[b]	HD 136418[b]	HD 212771[b]
Period (days)	356.0 (2.6)	507 (16)	663 (29)	610 (13)	479 (13)	464.3 (3.2)	373.3 (3.4)
T_p[a] (JD)	2454804 (80)	2454983 (90)	2454881 (50)	2454677 (20)	2454690 (130)	2455228 (10)	2454947 (40)
Eccentricity	0.041 (0.037)	0.157 (0.086)	0.177 (0.057)	0.229 (0.058)	0.09 (0.11)	0.255 (0.041)	<0.21
K (m s^{-1})	46.9 (1.9)	23.5 (1.9)	52.3 (3.7)	40.7 (1.9)	30.7 (3.7)	44.7 (1.9)	58.2 (7.8)
ω (deg)	76 (80)	317 (60)	281 (30)	296 (10)	300 (100)	12 (10)	55 (40)
$M_P \sin i$ ($M_{\rm Jup}$)	2.3 (0.2)	1.2 (0.1)	3.3 (0.2)	2.2 (0.1)	1.6 (0.2)	2.0 (0.1)	2.3 (0.4)
a (AU)	1.19 (0.03)	1.51 (0.05)	1.78 (0.07)	1.68 (0.05)	1.39 (0.04)	1.32 (0.03)	1.22 (0.03)
Linear trend (m s^{-1} yr^{-1})	0 (fixed)	30.9 (1.9)	0 (fixed)	0 (fixed)	135.4 (3.5)	-5.3 (1.7)	0 (fixed)
rms (m s^{-1})	3.7	5.7	4.7	4.8	3.3	5.0	5.8
Jitter (m s^{-1})	5.0	5.0	5.0	5.0	5.0	5.0	5.0
$\sqrt{\chi_\nu^2}$	0.79	1.32	1.14	1.06	0.98	1.15	1.29
$N_{\rm obs}$	29	22	17	24	12	25	20

[a] Time of periastron passage.

[b] In cases where the eccentricity is consistent with $e = 0$, we quote the 2σ upper limit from the MCMC analysis.

Bowler et al. (2010) found that the minimum masses and semi-major axes of planets around A stars are very different from those of planets around FGK stars. Their findings suggest that the formation and migration mechanisms of planets change dramatically with increasing stellar mass. The planets reported in this work strengthen that conclusion. The five new planets we have discovered around stars with $M_\star > 1.5\ M_\odot$ all orbit beyond 1 AU and have minimum masses $M_P \sin i > 1\ M_{\rm Jup}$. These properties contrast with those of planets orbiting less-massive stars, which have a nearly flat distribution in log a, from $a = 0.05$ AU to $a = 1$ AU (Cumming et al. 2008), and a steeply rising mass function with $d \ln N/d \ln M_P = -1.4$. Successful theories of the origin and orbital evolution of giant planets will need to account for the discontinuity between the distributions of orbital parameters for planets around Sun-like and A-type stars (Kennedy & Kenyon 2008; Currie 2009; Kretke et al. 2009).

The abundance of super Jupiters ($M_P \sin i > 1\ M_{\rm Jup}$) detected around massive stars bodes well for future direct-imaging surveys. In addition to harboring the massive planets that are predicted to be the most easily detectable in high-contrast images, A-type dwarfs have the added benefit of being naturally young. A $2\ M_\odot$ star has a main-sequence lifetime of only ~1 Gyr, which means that Jovian planets in wide orbits will be young and thermally bright. Three of the planets in Table 10 show linear velocity trends indicative of additional long-period companions. These linear trends provide clear markers of massive objects in wide orbits around nearby stars, and therefore warrant additional scrutiny from RV monitoring and high-contrast imaging.

REFERENCES

Artigau,É., et al. 2008, Proc. SPIE, 7014, 70141Z
Bowler,B. P., et al. 2010, ApJ, 709, 396
Brittain, S. D., Najita, R., J., & Carr, J. S. 2009, ApJ, 702, 85
Butler, R. P., et al. 1996, PASP, 108, 500
Claudi, R. U., et al. 2006, Proc. SPIE, 6269, 62692Y

Cumming, A., et al. 2004, MNRAS, 354, 1165
———. 2008, PASP, 120, 531
Currie, T. 2009, ApJ, 694, L171
Dodson-Robinson, S. E., et al. 2009, ApJ, 707, 79
Döllinger, M. P., et al. 2009, A&A, 505, 1311

Eaton, J. A., Henry, G. W., Fekel, F. C. 2003, in The Future of Small Telescopes in the New Millennium. Vol. II–The Telescopes We Use, ed. T. D. Oswalt, (Dordrecht: Kluwer) 189

Perryman, M. A. C., et al. 1997, A&A, 323, L49

Fischer, D. A., et al. 2003, ApJ, 586, 1394

Fischer, D. A., & Valenti, J. 2005, ApJ, 622, 1102

Fitzgerald, M. P., Kalas, P. G., & Graham, J. R. 2009, ApJ, 706, L41

Flower, P. J. 1996, ApJ, 469, 355

Ford, E. B. 2005, AJ, 129, 1706

Galland, F., et al. 2005, A&A, 443, 337

Gelman, A., Rubin, & B., D. 1992, Statistical Science, 7, 457

Girardi, L., et al. 2002, A&A, 391, 195

Hatzes, A. P., et al. 2003, ApJ, 599, 1383

Hekker, S., et al. 2006, A&A, 454, 943

Henry, G. W., et al. 1995a, ApJS, 97, 513

Henry, G. W., Fekel, F. C., & Hall, D. S. 1995b, AJ, 110, 2926

Henry, G. W., et al. 2000, ApJS, 130, 201

Hinkley, S., et al. 2008, Proc. SPIE, 7015, 701519

Howard, A. W., et al. 2009, ApJ, 696, 75

Ida, S., & Lin, D. N. C. 2005, Progr. Theor. Phys. Suppl., 158, 68

Isaacson, H. T. 2009, AAS, 41, 206

Johnson, J. A. 2009, PASP, 121, 309

Johnson, J. A., et al. 2007a, ApJ, 670, 833

———. 2007b, ApJ, 665, 785

———. 2010, PASP, 122, 149

———. 2006, ApJ, 652, 1724

———. 2008, ApJ, 675, 784

Kalas, P., et al. 2008, Science, 322, 1345

Kennedy, G. M., & Kenyon, S. J. 2008, ApJ, 673, 502

Kretke, K. A., et al. 2009, ApJ, 690, 407

Kuha, J. 2004, Sociol. Methods Res., 33, 188

Lafrenière, D., Jayawardhana, R., & van Kerkwijk, M. H. 2008, ApJ, 689, L153

Lagrange, A., Desort, M., & Meunier, N. 2010, preprint (arXiv:1001.1449)

Lagrange, A., et al. 2009a, A&A, 506, 927

Lagrange, A.-M., et al. 2009b, A&A, 493, L21

Liddle, A. R., et al. 2004, MNRAS, 351, L49

Lineweaver, C. H., & Grether, D. 2003, ApJ, 598, 1350

Liu, Y.-J., et al. 2008, ApJ, 672, 553

Lovis, C., & Mayor, M. 2007, ApJ, 472, 657

Macintosh, B. A., et al. 2008, Proc. SPIE, 7015, 701518

Makarov, V. V., et al. 2009, ApJ, 707, L73

Marcy, G., et al. 2005, Prog. Theor. Phys. Suppl., 158, 24

Marcy, G. W., & Butler, R. P. 1992, PASP, 104, 270

Marcy, G. W., et al. 2008, Phys. Scr. Vol. T, 130, 014001

Marois, C., et al. 2008, Science, 322, 1348

Niedzielski, A., et al. 2009, ApJ, 693, 276

———. 2007, ApJ, 669, 1354

Noyes, R. W., et al. 1984, ApJ, 279, 763

Paulson, D. B., et al. 2004, AJ, 127, 1644

Peek, K. M. G., et al. 2009, PASP, 121, 613

Queloz, D., et al. 2001, A&A, 379, 279

Quillen, A. C. 2006, MNRAS, 372, L14

Reffert, S., et al. 2006, ApJ, 652, 661

Saar, S. H., Butler, R. P., & Marcy, G. W. 1998, ApJ, 498, L153+

Sato, B., et al. 2005, ApJ, 633, 465

———. 2007, ApJ, 661, 527

———. 2008, PASJ, 60, 1317

Schwarz, G. 1978, Ann. Stat., 461

Setiawan, J., et al. 2005, A&A, 437, L31

Tabachnik, S., & Tremaine, S. 2002, MNRAS, 335, 151

Valenti, J. A., et al. 2009, ApJ, 702, 989

Valenti, J. A., & Fischer, D. A. 2005, ApJS, 159, 141

Valenti, J.A., & Piskunov, N. 1996, A&AS, 118, 595

van Leeuwen, F. 2007, A&A, 474, 653

Vogt, S. S., et al. 1994, Proc. SPIE, 2198, 362

Winn, J. N., Holman, M. J., & Fuentes, C. I. 2007, AJ, 133, 11

Wright, J.T. 2005, PASP, 117, 657

Wright, J. T., & Howard, A. W. 2009, ApJS, 182, 205

Wright, J. T., et al. 2004, ApJS, 152, 261

Wyatt, M. C., et al. 1999, ApJ, 527, 918

Yi, S. K., Demarque, P., Kim, & Y.-C. 2004, Ap&SS, 291, 261